Proton strings and rings in atypical nucleation of ferroelectricity in ice

J. Lasave,[1,2] S. Koval,[1] A. Laio,[2,3] and E. Tosatti[2,3]

[1] *Instituto de Física Rosario, CONICET and Universidad Nacional de Rosario, 27 de Febrero 210 Bis, 2000 Rosario, Argentina*
[2] *International Center for Theoretical Physics (ICTP), Strada Costiera 11, I-34151 Trieste, Italy*
[3] *International School for Advanced Studies (SISSA), and CNR-IOM Democritos, Via Bonomea 265, I-34136 Trieste, Italy*

(Dated: January 1, 2021)

Ordinary ice has a proton-disordered phase which is kinetically metastable, unable to reach spontaneously the ferroelectric (FE) ground state at low temperature where a residual Pauling entropy persists. Upon light doping with KOH at low temperature the transition to FE ice takes place, but its microscopic mechanism still needs clarification. We introduce a lattice model based on dipolar interactions plus a competing, frustrating term that enforces the ice rule (IR). In the absence of IR-breaking defects, standard Monte Carlo (MC) simulation leaves this ice model stuck in a state of disordered proton ring configurations with the correct Pauling entropy. A replica-exchange accelerated MC sampling strategy succeeds, without open path moves, interfaces or off-lattice configurations, to equilibrate this defect-free ice, reaching its low-temperature FE order through a well defined first order phase transition. When proton vacancies mimicking the KOH impurities are planted into the IR-conserving lattice, they enable standard MC simulation to work, revealing the kinetics of evolution of ice from proton disorder to partial FE order below the transition temperature. Replacing ordinary nucleation, each impurity opens up a proton ring generating a linear string, an actual ferroelectric hydrogen-bond wire that expands with time. Reminiscent of those described for spin ice, these impurity-induced strings are proposed to exist in doped water ice too, where IRs are even stronger. The emerging mechanism yields a dependence of the long time FE order fraction upon dopant concentration, and upon quenching temperature, that compares favorably with that known in real life KOH doped ice.

PACS numbers:

I. INTRODUCTION

Ice famously intrigues experimentalists and theoreticians alike. The crystal structure of ordinary I_h ice consists of hexagonal rings of water molecules, each molecule tetrahedrally hydrogen-bonded to other four. Every proton occupies one of two sites along the H-bonds between two oxygens, and each oxygen satisfies the ice rule (IR), with two incoming and two ongoing H-bonds[1,2]. At low temperatures and under ordinary conditions, protons are unable to reach equilibrium, and ice is kinetically stuck in a glassy state characterized by the celebrated Pauling entropy[3,4] resulting from an infinity of different, IR-conserving, defect free proton configurations. Still debated is the possibility to attain, in pure ice at low T, the low energy, zero-entropy ferroelectric (FE) phase, ice XI, endowed with a macroscopic polarization order parameter, the protons occupying bond sites in a unique order. An intimate understanding of the possible FE ordering mechanism of pure ice is necessary in order to understand why and how it is avoided or reached. Of fundamental importance, that issue also bears potential implications in fields as disparate as astrophysics[5,6] and surface science[7,8].

The well known extrinsic ingredient which experimentally permits realization of ferroelectricity in bulk ice is KOH-doping, which allows ice to undergo, upon cooling below $T_c \approx 72$K[9], the transition from proton disorder to proton-ordered ferroelectricity. This transition has several remarkable features. First, its temperature is practically independent of the concentration and even of dopant type, suggesting the FE phase and its onset are in fact intrinsic equilibrium features of ice, escaping realization merely due to kinetic reasons when doping is absent[10]. Second, the ferroelectric order achieved after long annealing times is partial and its fraction depends weakly on the dopant concentration in a wide range[11]. Third, the transition kinetics upon quenching is significantly dependent on the quenching temperature T_q[12,13]. For example, at $T_q = 0.75T_c$ no ordering is observed, but at $T_q = 0.89T_c$ a fraction of the FE phase appears. As a simplifying note, we mention that nuclear quantum effects, generally relevant to hydrogen-bonded systems[14], may be provisionally neglected here, since deuteration affects only modestly the transition temperature[13,15].

The bulk of these observations is rationalized by the understanding that an FE state of low temperature hexagonal ice is thermodynamically favored, but its realization is hindered by a kinetic slowdown, likely due to the IR. The slowdown is overcome only in special conditions such as doping, accompanied by quenching from a sufficiently high T and subsequent annealing. Moreover, in many conditions the transition to the FE phase is incomplete, indicating that the slowdown mechanism can act also at the mesoscale. To physically clarify this scenario, it is desirable, due to the complexity of the problem, to resort to some simplified and yet microscopic model. The model should offer a comprehensive descrip-

tion of the non-ergodic proton disorder, of the ordered FE state, of their properties and ideal phase transition. It should also allow the introduction of dopants, with access to the transformation kinetics to partial FE ordering which they permit.

Microscopic model descriptions of ice are abundant, including off-lattice descriptions, both force-field based, such as Ref. [16] and ab initio. In particular, density functional theory (DFT) calculations also using graph invariants predict the existence of an FE transition at T_c=98K in pure hexagonal ice[17]. A better estimation of T_c ≈70-80K was obtained by recent DFT-based Monte Carlo (MC) simulations using hybrid functionals[18]. An FE ordered phase is also predicted in cubic ice by ab initio calculations, and is comparable in energy to the corresponding FE phase of hexagonal ice[19]. A recent study compares measured infrared spectra with theoretical results from classical molecular dynamics and ab initio simulations suggesting evidence of partial FE proton ordering in cubic ice[20]. A possible FE transition at low T in pure hexagonal ice was studied by lattice models using empirical water potentials, yet with relatively inconclusive results owing to strong dependence upon details of the potential models[21,22]. Alternatively, MC ice simulations using a point charge lattice model led to a nonferroelectric state at low T[23] but it was argued that the failure to find an FE state could be due to the simplifications of the model. In addition, many specific observations have been made concerning the importance of rotational Bjerrum defects[3], the role of Coulomb[24,25], of multipolar interactions[26], and other aspects[27,28] including off-lattice hydroxide configurations[29].

None of these realistic off-lattice concepts and considerations, however, seems so far to lead to a well defined model description of the subtle kinetic phenomena connected with establishing partial FE order, or the lack of it due to persistent and glassy proton disorder, formidable problems that a simplified lattice model is more likely be able to tackle. That calls therefore for a fresh attempt.

We have developed a bare-bone lattice model of ice, and a MC technique which allows simulating large samples at arbitrarily low temperatures (see *Calculation Details*). The main feature of this model is that while embodying "dipole-dipole" interactions, its finite temperature ensemble contains only configurations which satisfy exactly the IR. Even if a lower energy FE state is stabilized by dipolar interactions, standard MC fails to evolve configurations of this system even at finite temperature, causing it to retain the statistical distribution of proton rings and the Pauling entropy down to arbitrarily low temperatures, as in real neat ice. This ice-rule obeying disordered state provides an ideal framework where the effect on kinetics of an added idealized dopant can be studied.

The physics of our ice model, built on a diamond lattice, bears similarities to that of spin ice in pyrochlores, whose lattice is dual to diamond, making the two isomorphic upon identification of the orientation of the spins with the location of hydrogen atoms on the bonds between oxygens[30]. Unlike spin ice models our model "water oxygens" possess interacting dipoles whereas the only interaction between hydrogens ("spins") come from the topological ice-rule constraints. These analogies and differences underpin those that will appear in the equilibrium phase diagram, reminiscent but not identical to the 3D Kasteleyn transition[31] of spin ice in a field[32,33], as well as to the out-of-equilibrium, proton ordering behaviour. The kinetic process by which the dopant triggers proton ordering is an avalanche of proton hoppings, which breaking up closed rings, generate strings of collinear hydrogen bonds, all pointing in the same direction along a winding line, thus upsetting the ring landscape of the disordered phase. The barrier characterizing this simple process, which is of the order of the dipolar interaction, is therefore the rate limiting step for the formation of the string in ice.

Before introducing the details of our work, it should be stressed that our model study omits, by deliberate choice, many details that are known to play a role in real ice. In spite of that, we shall nonetheless throughout the paper compare the model's main results with known experimental facts. Points of agreement and disagreement between them will gauge the model's ability to address mechanisms that underlie some of the unexplained behaviors of ice ferroelectricity. In particular we will show that the string formation qualitatively reproduces several known facts in real KOH doped ice, providing bare-bone mechanisms for the dependence of the ferroelectric fraction on the dopant molar concentration, and on the quenching temperature.

II. MODEL

Our model system is a diamond lattice of N "water molecules" where each oxygen is connected tetrahedrally with four neighboring ones by H-bonds, as sketched in Fig. 1(a). This is the connectivity of cubic ice I_c. The cubic and hexagonal (I_h) phases of ice differ by the stacking order of the hexagonal bilayers that form the lattice, but their topologies are similar[19]. Since the model Hamiltonian, which is presented below, depends on the connectivity of the lattice sites but not on the distance between particles, the results obtained here should be valid for both I_c and I_h.

Each oxygen at site i in the diamond lattice has four bonds to nearby sites labeled by j. The variables of our model are the proton configurations on all bonds. We represent them by a set of $4N$ variables φ_{ij}, one for each *directed* bond. We have $\varphi_{ij} = 1$ if in that bond there is a proton closer to oxygen i and $\varphi_{ij} = -1$ if not. Note that in general φ_{ji} is independent from φ_{ij}. In pure ice, where we exclude Bjerrum defects[34], all bonds possess one and only one proton, and all oxygens two protons, $\varphi_{ij} = -\varphi_{ji}$, and the independent variable number shrinks to $2N$. A bond Ising-type variable $\vec{\sigma}_i^j$ is

defined as: $\vec{\sigma}_i^j = \varphi_{ij}\vec{e}_{ij}$, where $\vec{e}_{ij}$ is a vector pointing from oxygen site i to site j. Using these variables we define the dipole associated with oxygen site i as: $\vec{d}_i = \sum_j \varphi_{ij}\vec{e}_{ij} = \sum_j \vec{\sigma}_i^j$. That definition corresponds to a dipole of modulus one in each site satisfying the IR but is also valid for sites where it is not satisfied, where the dipole moduli are now smaller than one.

The Hamiltonian of our model is

$$H = -J \sum_{(i,j)_{nn}} \vec{d}_i \cdot \vec{d}_j + k \sum_{i=1}^{N} (\sum_{j(i)=1,...4} \varphi_{ij})^2, \quad (1)$$

where the two control parameters, J and k, are both positive. The first term represents the nearest-neighbor (nn) dipole-dipole ferroelectric interaction between oxygen tetrahedra. The second term penalizes configurations that violate the IRs. Indeed, $\sum_j \varphi_{ij} = 0$ only if two protons are close to site i and two are far.

We will mostly describe the properties of this model, which to the best of our knowledge has not been studied for ice, in the special case $k \to \infty$, where violations of the IR are forbidden. Yet, we will make use of finite k in replica-exchange accelerated MC. The physical order parameter is the FE polarization, defined as

$$\vec{P} = \frac{1}{N} \sum_{i=1}^{N} \vec{d}_i. \quad (2)$$

The model can be mapped, translating from site to bond variables, to an Ising-type Hamiltonian

$$H = -(J+k) \sum_{(il,jm)_{nn}} \vec{\sigma}_i^l \cdot \vec{\sigma}_j^m - J \sum_{(il,jm)_{nnn}} \vec{\sigma}_i^l \cdot \vec{\sigma}_j^m. \quad (3)$$

The first term is a large (practically infinite) ferroelectric coupling between nearest neighbor bonds, promoting frustration and disorder through its strong topological IR constraints. That effect is mitigated by the second term, also ferroelectric, between second neighbor bonds, contributing instead to stabilize a possible FE ordered state at low T.

It should be noted that off-lattice configurations[29] as well as multipolar terms and long-range interactions[24–28], are omitted. Testing the effects of removing these drastic approximations is beyond the scopes of this first study. Mainly justified by simplicity, the short-range interaction assumption is at least encouraged by screening of long-range electrostatic tails, which is induced by polarization. It may also be noted that, unlike first neighbor interactions, always ferroelectric, the sign of long-range interactions is not uniform, but rather oscillates between ferro and antiferro depending on direction, suggesting a certain level of cancellation. Indeed, MC studies of the dipolar spin ice model actually showed that medium to long range interactions are screened out, suggesting that short range physics should remain qualitatively valid[30,35–37].

The KOH impurities, which play a fundamental role in determining the kinetics, are introduced in our model as follows. In ice the K^+ impurity replaces a proton in one bond. This turns the proton-deficient molecule into a cation-hydroxide pair $K^+(OH)^-$. That is simulated in our model by a single, fixed proton vacancy in a bond ij (represented by setting $\varphi_{ij} = \varphi_{ji} = -1$), an action which simultaneously deprives oxygen site i of an outgoing proton, (this is the Bjerrum defect mimicking K^+, which we keep fixed), and deprives oxygen site j by one incoming proton – this is a mobile IR breaking defect, mimicking $(OH)^-$. We have no charges in our model, but for the sake of illustration, we will call these two defects K^+ and OH^-. The presence of charge dopants in real doped ice induces lattice distortion, which could lower the relaxation barrier of the local structure, speeding the interconversion from paraelectric (PE) to FE. However, the formulation of our model does not allow assessing how important this particular effect is.

III. CALCULATION DETAILS

We carried out MC simulations on a diamond lattice with 12x12x12 cubic cells containing $N = 13824$ sites, representative of static oxygen sites in cubic ice. A z-directed electric field is coupled to the polarization for breaking the symmetry of the isotropic Hamiltonian. The field is removed after equilibration and is small enough ($|\vec{E}| \approx J/10$) in order not to modify the transition temperature. First of all we confirmed that the IR term causes frustration that prevents our defect free ice model from reaching thermodynamic equilibrium within standard MC sampling, where proton variables φ_{ij} change one at a time while chosen randomly through the lattice. $2N$ proton move attempts performed sequentially represent our MC step or pass. This well known problem was addressed long ago by Rahman and Stillinger[2] who dealt with the IR by performing random walks on the lattice and noticing that paths involving crossing of the periodic boundaries bring in a change in total dipole moment. Time-honored as it is, that method involves the necessity of very large simulation sizes, which we prefer to avoid. We thermalize the system by a Hamiltonian Replica Exchange Method (HREM)[38]. We simulated $m = 1, 2, ...M$ replicas in parallel, at the same temperature and same J but with different values of the ice-rule penalty parameter k. The original replica $m = 1$ has a prohibitively large value of $k = 30J$, practically infinite. As m increases the parameter k is reduced successively until the last replica $m = M = 40$, which corresponds to $k = 0$. The IR-violating defects (excess or lack of protons attached to an oxygen site) will therefore occur with increasing probability in replicas with decreasing k. After a prescribed number of MC steps the instantaneous configurations for adjacent replica are allowed to swap with a probability dictated by the standard Metropolis exchange criterion[39,40].

As a direct extension of the intrinsic, defect free model, whose equilibrium properties will be shown to agree well

with those of pure ice, we subsequently introduced defects, and studied the kinetics which they generate. This is done in a lattice of 9x9x9 cubic cells containing 5832 sites. To represent the effect of "KOH type" impurities, a small number of $L \ll N$ fixed proton vacancies were introduced, randomly distributed in lattice bonds ij, by setting $\varphi_{ij} = \varphi_{ji} = -1$, i.e. no proton either near oxygen i or near oxygen j, as if it had been moved to the nearby interstice in order to mimic the role of K^{+3}. In Fig. 3 the proton vacancy in a given bond is depicted by an interstitial K^+ ion schematically replacing the proton H^+. In real ice, the KOH impurity produces two mobile defects: an ionic OH^- defect and a Bjerrum $L-$defect (proton vacancy)[3]. In our model, for the sake of simplicity, the Bjerrum $L-$defect is fixed and only the hydroxide defect is able to move. Thus, the introduced impurity generates a traveling hydroxide which can trigger transitions involving the nearby protons, transitions otherwise impossible (see Fig. 3(b)). It's worth noting here that we expect similar kinetic effects from a mobile Bjerrum $L-$defect as those observed with a traveling hydroxide.

To address the kinetics of the doped ice model, we performed non-equilibrium simulations by a quenching-annealing (QA) simulation protocol, carried out with standard MC moves – which mimicks to some extent the real time evolution of experiments – and by comparison also with the HREM protocol, which artificially speeds up evolution towards equilibrium. Each calculation performed was an average of 50 runs with different random-number generator seeds. Starting with the doped system initially thermalized with HREM at very high $T \sim 3$ T_c, we quench it down to a temperature T_q below T_c (quenching) and then let it thermalize at the quenching temperature T_q till the system comes as close as possible to equilibrium (the annealing process). That was done for a range of T_q and of doping concentrations, so as to address the known experimental dependence of ice ferroelectricity upon these parameters.

IV. RESULTS

A. Equilibrium phase diagram and proton rings

We first discuss the equilibrium phase diagram for defect-free bulk ice model, where no violations to the IR are allowed. In order to thermalize this model we use a Hamiltonian Replica Exchange Method (HREM) (see *Calculation Details*), in which a set of replicas differing only by the IR-controlling parameter k, are simulated in parallel. In the first replica k is extremely large, as appropriate to the IR conserving model we want to address, in the other replicas k is succesively smaller and smaller. Configurations of different replicas are exchanged according to a replica exchange protocol, which allows the simultaneous thermalization of all the replicas. Fig. 1(d), shows the average value of the polarization P as a function of temperature. There is a transition between an ordered FE state ($P \sim 1$) and a disordered PE state ($P \sim 0$) at an equilibrium transition temperature $T_c \approx 3J$. As expected, T_c is proportional to the strength of the oxygen dipolar-interaction parameter J (see Eq. 1). The transition appears to be strongly first order. Even without the IR constraint (k=0), the symmetry-dictated universality class of this transition would differ from straight Ising. Indeed, the Hamiltonian (Eq. 1) possesses six equivalent FE ground states (polarization along x, -x; y, -y; z, -z), making it closer (yet not identical) to a Potts model, a family many members of which support first order phase transitions in high dimensions (see e.g. Ref.[41]). Conversely, the fully IR conserving Hamiltonian would, once the dipole-dipole interaction was removed (J=0) and the protons were coupled to an electric field, display a Kasteleyn-type transition[31] as in spin ices. With nonzero J and large k, our model is richer, even if retaining some qualitative similarities to Potts and Kasteleyn transitions. A note of caution here is that while the experimental FE transition of real ice is, as in this model, first order[3,5], there are in ice secondary order parameters, such as strain coupling, that are absent in the model but that would play a role making the transition first order.

Next, the equilibrium entropy evolution with temperature is a crucial information. We obtain it at each temperature as the integral of the specific heat at constant volume over T. Strictly speaking, this procedure is correct only if no first-order phase transitions are encountered along the path. However, in finite size systems like those analyzed in this work, first order transitions are avoided, the thermodynamic potentials vary continuously, and the procedure is therefore justified. The inset of Fig. 1(d) shows how at T_c the entropy of the defect free IR conserving model correctly rises from essentially zero (the model has no acoustical modes) to the Pauling value $S \sim \ln(3/2)$ across the transition. The free energy F as a function of the polarization can be estimated, at a given temperature, from the histogram of the polarization observed in the first replica. F is shown in Fig. 1(c). At T_c, F shows two minima with same free energy separated by a barrier, which confirms the first-order character of the transition. At $T = 0.93T_c$ the free energy retains a secondary minimum at $P \sim 0$, signaling a metastable (equilibrated) PE state which, however, no longer exists at $T = 0.85T_c$. An analogous metastable FE state must also exist above T_c, but is already lost at $T \sim 1.03T_c$. Thus, free-energy barriers vanish shortly below and just above T_c. Associated with the transition there is a change in the proton configuration inside the 12 hexagonal rings which thread each lattice site. The role of rings and directed H-bonds is widely discussed in ice and water[16,43]. Here, we must in addition distinguish different ring types according to their polarization. For that, we associate an arrow to each H-bond, pointing from the oxygen possessing a close-by proton to the other oxygen in that bond (see Fig. 1(e)). We then count, for each ring, the number of arrows pointing in a specific

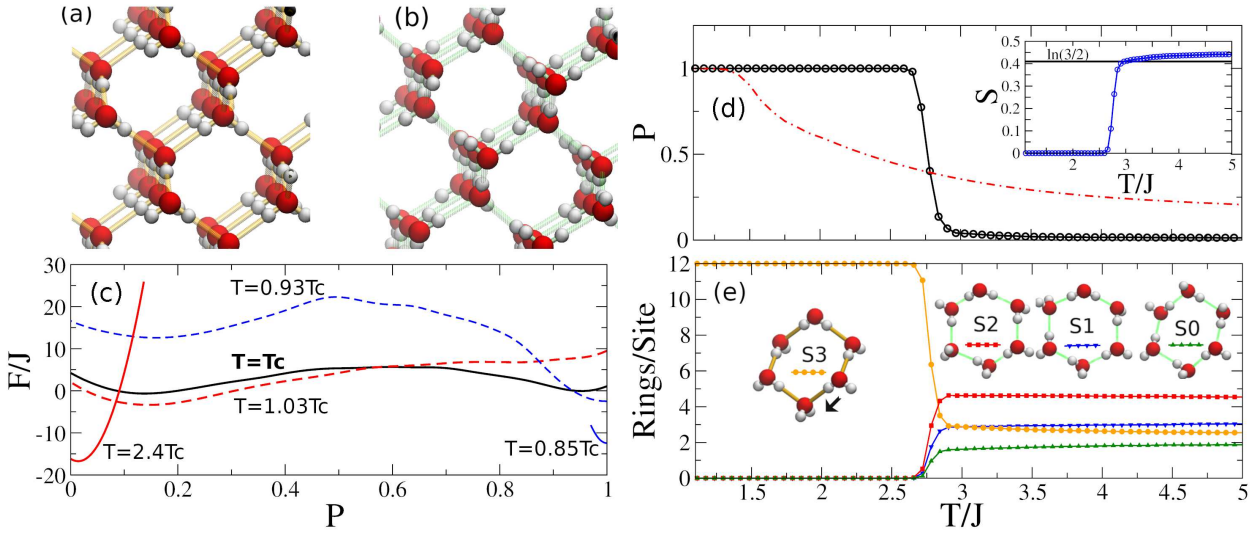

Figure 1: (a) Simulation snapshot showing the FE order in ice at $T < T_c$. (b) Simulation snapshot showing a characteristic PE configuration in ice at $T > T_c$. (c) Free energy F in units of the coupling constant J as a function of polarization P for different temperatures. The FE ($P \sim 1$) and PE ($P \sim 0$) minima at T_c are separated by a barrier, consistent with a first order transition. (d) Equilibrium averaged polarization P vs temperature in units of J obtained by HREM for the model of Eq. 1 (black solid line and empty circles). Red dotted-dashed line: Kasteleyn-like polarization as a function of $T/|\vec{E}|$ for a spin-ice model [42] with the same IRs as in Eq. 1, but $J = 0$ and with z-oriented electric-field $\vec{E}$ coupled to dipoles $(-\vec{d}.\vec{E})$. Inset: entropy in units of the Boltzmann constant vs T/J for our ice model (blue line and empty circles). The horizontal solid line indicates the value of the Pauling entropy, which actually persists down to low T in ordinary MC simulations. (e) Hexagonal ring population vs temperature in units of J. The insets show schematically the proton arrangements for the different type of rings: S_0, S_1, S_2 and S_3. We also show the arrow associated to a given configuration of an O-H-O bond in the ring S_3, which is defined for computing the ring-order parameter s (see *Equilibrium Phase Diagram and Proton Rings*).

clockwise direction, and define from that a directed order parameter $s = (6 - |\sum_{i=1}^{6} \varphi_{il}|)/2$, where i runs through the six-site ring clockwise, $l = i + 1$, and φ_{il} is the proton variable of the H-bond il. The four different kinds of proton rings are schematically depicted in Fig. 1(e) labeled as S_s, therefore S_3, S_2, S_1, and S_0, corresponding to $s = 3, 2, 1$ and 0, respectively. This ring classification differs from a previous one (see Supp. Inf. of Ref. [43]), except for the case of the ring S_0.

A schematic representation of a typical microscopic configuration in the PE phase of ice is depicted in Fig. 1(b). Inspecting all hexagonal rings in the equilibrium state of the defect-free ice model, we extract the average population $< n_s >$ of rings of each $s = 0, ..3$. Fig. 1(e) shows the results obtained as a function of temperature. For each site $\sum_s^3 < n_s >= 12$ in pure ice at all temperatures. Well below T_c, all rings have $s = 3$, thus $n_3 = 12$, accompanied by a net local polarization along z. In this FE state, schematically displayed in Fig. 1(a), where only z-polarized S_3 rings are present, the symmetry between the six possible polarizations of the system (along the x, y or z axis, and corresponding negative directions) is spontaneously broken by long-range order. At T_c, $< n_3 >$ has a sharp drop which accompanies the collapse of the order parameter P, while all other rings concurrently surge and proliferate as shown in Fig. 1(e). Finally, in the PE phase above T_c, all ring populations acquire steady values, almost constant with further temperature increase. The S_3 rings do not disappear, but we find them equally polarized in all directions in accordance with the vanishing order parameter. In the following, S_2, S_1, and S_0 are called "disordered" rings because they only appear in the disordered phase. The slight residual temperature dependence can be attributed to finite size in our simulations.

Entropy reveals another effect of small size. Our calculated entropy at $T > T_c$ is $\approx 10\%$ higher than the Pauling entropy as shown in the inset of Fig. 1(d). Pauling's entropy is known to be only a lower bound[33]. Our HREM calculations capture the additional proton correlations along the closed rings, which cause entropy to rise higher for smaller sizes[44].

The population distribution of rings in the disordered phase is also similar to that found in a recent ab initio molecular dynamics study of hexagonal ice[43]. For instance, the relative abundance of S_0 rings is about 15.8% in our calculation which is nearly equal to the corresponding averaged-value obtained in Ref.[43] for hexagonal ice, $\approx 16.5\%$.

B. Non-equilibrium kinetics and FE polarization in doped ice

Thus far we described the static properties, both equilibrium and metastable, of the ice model. It is now possible to address the nonequilibrium MC kinetics of transformation between PE and FE states. The equilibrium transition being first order, the transformation will occur by nucleation. Yet, this process is very strongly influenced by IR constraints, which render ordinary homogeneous nucleation impossible, at least for k large enough. In that limit, only inhomogeneous nucleation is possible. We therefore study the transformation from the metastable and proton disordered state, into an ordered or partly ordered FE state, taking place once model impurities, meant to play a similar role to KOH, are introduced. To that end, we first equilibrate with HREM the IR conserving state at high $T \sim 3T_c$, and then quench it down to some T_q below T_c where we let it thermalize with standard MC moves. We call this procedure a quenching-annealing (QA) simulation protocol (see *Calculation Details*).

Initially, after a certain number of thermalization time steps at high T, the system reaches a state where all the ionic defects (hydronium - hydroxide pairs and even molecular states with zero or four protons) introduced by the random initial configurations managed to recombine and disappear. We checked that after thermalization at high T in the KOH-doped system with L extrinsic impurities, we have precisely L mobile hydroxide defects in the system because all intrinsic ionic defects permitted by finite k have recombined (see Fig. 3). After equilibration at high T with HREM, all the simulations continue with a QA protocol using standard MC (unless otherwise stated) on the replica with the largest k value. Fig. 2(a) shows the non-equilibrium evolution of the instantaneous polarization in a QA simulation after quenching at $T_q = 0.57T_c$, in a range of different conditions. As a first check, in pure ice ($L = 0$) the system remains stuck in a non-equilibrium glassy state with $P \ll 1$ as shown by the blue dashed curve in Fig. 2(a). If HREM is instead kept active throughout, then the low-temperature thermodynamic equilibrium with $P = 1$ (FE order) is quickly recovered after quenching, as expected and as shown by the green curve in Fig. 2(a).

The next step is the simulation of doped ice with L impurities representing KOH impurities (see *Model* and *Calculation Details*). Unlike the undoped case ($L = 0$), results for $L = 1$, 4, and 8, show a kinetic evolution with frank onset of the FE order parameter (see Fig. 2(a)). At large MC step number (conventionally representing long evolution times), the polarization P reaches $\approx 60 - 75\%$, almost independent of the impurity number L. This is in qualitative agreement with neutron diffraction measurements of doped deuterated ice, where a volume abundance of $\approx 48\%$ of ice XI is observed in the bulk at $T = 0.89T_c^{exp}$[12]. The critical temperature and the ice XI fraction locally formed are practically independent of the impurity concentration[9–11,13,45], a nontrivial outcome which is reproduced by our model. The $L = 1$ case corresponds to a molar fraction of 1/5832, similar to that of the doped-ice samples used in Ref.[10], 1/5540, and leads to extensive FE ordering in the model that is qualitatively similar to experiment[9,10,12]. Moreover, neutron diffraction of annealed KOD-doped deuterated ice after low T quenching showed a sustained intensity growth of the characteristic 131-Bragg peak of the FE phase XI. Its intensity, proportional to the volume fraction of ferroelectric ice-XI, tends to a definite limit at long annealing times[12], also decreasing when the quench temperature was lowered, as shown in Fig. 2(c). We conducted additional extensive weak-doping simulations, with $L = 1$, exploring how a change of T_q affects the kinetics of FE onset. As Fig. 2(b) shows, the calculated long-time FE fraction diminishes as the quenching temperature is lowered, in qualitative agreement with the neutron diffraction data of Fig. 2(c). There are therefore good hopes that our model could shed light on the underlying reasons.

C. Microscopic mechanism of string nucleation

We now analyze the microscopic mechanism of IR defect-induced disorder nucleation in the FE phase and conversely, the impurity-induced nucleation and growth of FE clusters in the PE phase. First, we address the impurity-triggered nucleation of disorder by regular MC simulations of an ordered FE crystal at $T = T_c/2$. At this low temperature, as shown in Fig. 3(a), the hydroxide is unable to propagate freely through the crystal. However, when temperature rises above T_c ($\approx 2T_c$), the hydroxide departs from the impurity site, and travels through the lattice (see Fig. 3(b)). In its journey, it flips onto the xy plane the dipoles from their original FE z-polarization. That generates a chain, or string, of xy-dipoles, shown by the blue line in Fig. 3(b), with origin in the fixed initial impurity site and end at the moving hydroxide. This chain bears a resemblance to the so-called "Dirac" string associated with a magnetic monopole of model spin ice systems[46–48]. While the IR is of course the topological constraint that water ice and spin ice have in common which gives rise to strings in both cases, the two model systems are far from identical, as we will underline later.

As shown in Figs. 3(a) and 3(b), in the early stages of string formation the hydroxide can only progress upwards (see the blue path) along z and against the total polarization. As the ice rules are satisfied everywhere and the system is in the ordered phase, it can only receive one of the two protons from the top neighbouring water molecules. The preference will be to receive the one that creates locally a basal dipole aligned to that of the previous step in the hydroxide path, thus creating a chain of dipoles aligned in the x or y directions, no longer along z. This has an energy cost of $\Delta E = 2J$ per step. Otherwise, the resulting basal dipole would be perpen-

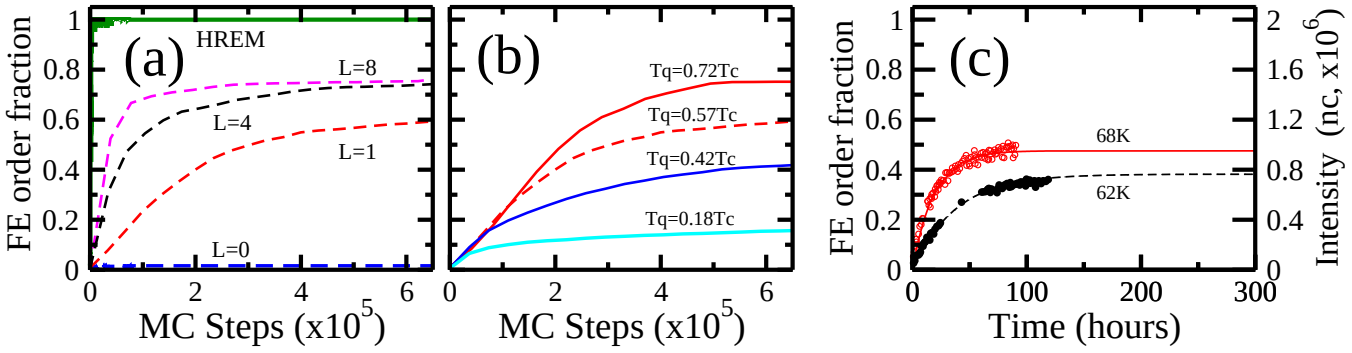

Figure 2: (a), (b) FE order fraction (or equivalently, instantaneous polarization) attained after quenching vs the number of MC steps. (a) FE fraction for a quenching temperature $T_q = 0.57T_c$ and different number L of impurities. For $L = 0$, we show with blue dashed line the regular MC results and with green solid line the HREM results. Regular MC results for $L = 1$, 4, and 8 (molar fractions 1/5832, 4/5832 and 8/5832, respectively) are shown with red dashed line, black dashed line and magenta dashed line, respectively. (b) Regular MC results for $L = 1$ (molar fraction 1/5832) and different quenching temperatures. Results for $T_q = 0.18T_c$, $0.42T_c$, $0.57T_c$, and $0.72T_c$ are shown with turquoise solid line, blue solid line, red dashed line, and red solid line, respectively. (c) Evolution with time of the 131-Bragg peak neutron count (nc, right ordinate) obtained in diffraction experiments of KOD-doped deuterated ice[12]. Solid black (open red) circles are from the same sample once annealed at $T =$ 62 (68) K. Left ordinate: corresponding ice-XI mass fraction (a measure of FE order, proportional to Bragg intensity) for the sample annealed at $T = 62$ K (black dashed line) and 68 K (red solid line), after Ref.[12].

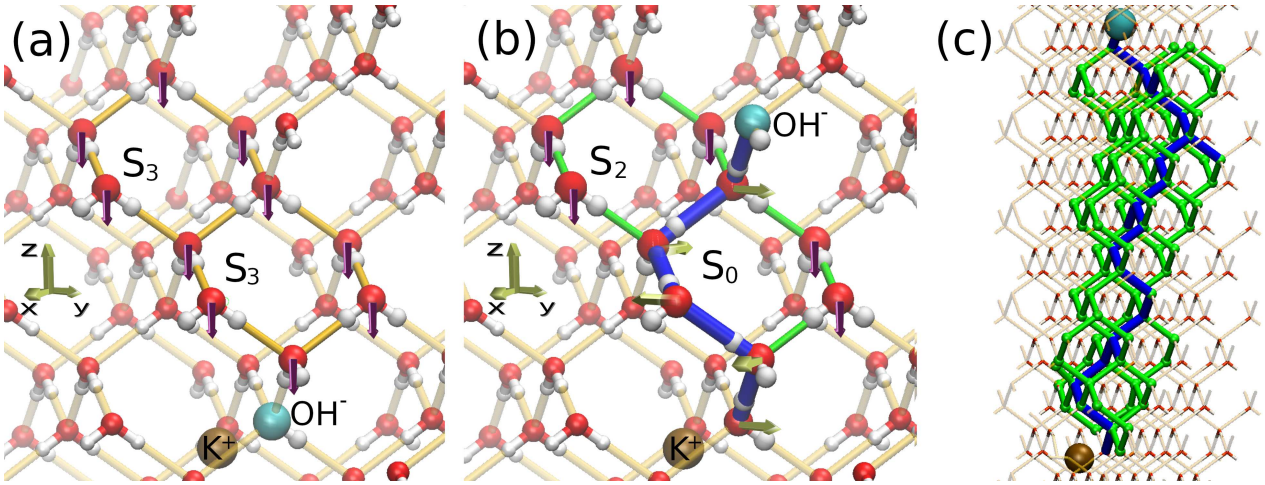

Figure 3: Nucleation mechanism of disorder in the ordered FE phase of ice depicted with snapshots of the simulation at different stages of the process (see explanations in *Microscopic Mechanism of String Nucleation*): (a) in the doped FE phase at $T = T_c/2$ with the characteristic S_3 rings colored with mustard. The planted proton vacancy representing the doping by a KOH impurity produces a hydroxide defect (colored with turquoise) which remains in its site at this simulation temperature. Notice that we added a fixed K^+ atom colored with brown next to the proton vacancy for the sake of clarity in the picture as explained in *Calculation Details* (see also *Microscopic Mechanism of String Nucleation*); (b) immediately after the suddenly raise of T above T_c showing the hydroxide displacement through single proton jumps following the blue path and transforming two z-polarized mustard rings S_3 into two "disordered" green rings S_0 and S_2; (c) after a longer simulation time above T_c showing the creation of a PE cluster (green rings) along the blue path of the hydroxide. Violet (green) arrows at different oxygens represent z-polarized (xy-polarized) dipoles $\vec{d}_i$.

dicular to that of the previous step with a higher cost $\Delta E = 3J$. Yet, since MC moves are randomly generated and accepted according to Boltzmann weights, the chain-end hydroxide progresses, owing to finite temperature, not only in the z direction but also in the x or y directions, as in Figs. 3(b) and 3(c). As noted, the disordering mechanism produced onto the initially perfect FE system by the hydroxide string with a probability that bifurcates at each step along the path resembles that of the three-dimensional Kasteleyn-like transition of spin ice in external field[49]. However, in our ice model the transition is not induced globally by an external field, but by the J-induced local field created by the growing seed. Unlike Kasteleyn's strict case of spin ice models,

where an infinite number of configurations are degenerate and excitations have a large gap[30], here nucleation brings the system closer to a lower free energy state due to the local dipole-dipole interactions. A second difference is that the local dipole field makes the probability to move a proton in the two possible branches uneven, affecting qualitatively the nucleation dynamics.

The disorder produced by the hydroxide migration may also be characterized by the transformation of z-polarized S_3 (mustard) rings into S_2, S_1 or S_0 (green) "disordered" rings with a certain degree of xy-polarization (see also Fig. 1). For instance, Fig. 3(b) shows the formation of an S_0 ring with a three-step hydroxide jump, and that of an S_2 ring with a single-step jump. Thus, the traveling hydroxide nucleates in its path a disorder "contagion" cloud, formed by green rings, elongated in the z direction and zigzagging in the x and y directions, as shown in Fig. 3(c). The green cluster shown in this figure has a substantially smaller polarization than the FE bulk, and can thus be considered a seed of the PE phase inside the FE bulk. It is worth noting here that after the hydroxide has passed, the green PE cluster cannot further spread expanding its frontier perpendicularly to the blue line because the strong IR constraints frustrate any proton move attemp across the cluster boundary during the standard MC simulation, as they presumably would in real time evolution. In other words, the PE cluster can only progress as an elongated string through the traveling-hydroxide tip.

In reverse, and crucially, we finally address the nucleation mechanism of FE order inside the disordered phase. Thermalizing the system with a single impurity ($L = 1$) at a high $T = 3T_c$, with an initial HREM MC simulation lasting 20000 steps, we choose the replica with the largest k value, therefore with well-respected IRs. With that, a regular (Metropolis) MC simulation is continued for the same number of steps. In this thermalization, the hydroxide migrates following a completely random path and losing track of the initial impurity site. Fig. 4(a) shows a typical configuration formed after thermalization. Completely disordered, it displays all types of S_β rings as described earlier. This disordered configuration is then suddenly quenched to a low temperature below T_c (see Figs. 4(b) and 4(c)). The reduced mobility of the hydroxide and the decrease of entropic contributions in favor of enthalpic ones reflects in the tendency of the hydroxide to migrate preferentially in one direction, that will in fact define the incipient polarization direction which we denote as z, as in Figs. 4(b) and 4(c). In its way along the new path, the hydroxide transforms disordered green rings into ordered z-polarized mustard ones. For instance, Figs. 4(a) and 4(b) show the transformation of a S_0 into a z-polarized S_3 ring as the hydroxide progresses along the blue path. This is precisely the reverse process to that displayed in Figs. 3(a) and 3(b). In its journey, the hydroxide may also take some steps that do not transform disordered rings into S_3 ordered ones, changing disordered rings into other disordered ones. Alternatively, this quenched evolution may also enlarge an existing ordered cluster by expanding its frontier, where again disordered rings turn into S_3 ones. All three possibilities were observed and appear in the snapshot taken from the simulation of Fig. 4(c). The net total result is the nucleation of ordered mustard rings along the blue path of the hydroxide.

V. DISCUSSION

We have described how FE and PE states transform into one another in a bare bone lattice model of ice, where only IRs and near-neighbor dipolar interactions are retained.

This model, it should be clear, has no ambition of describing real water ice in all chemical details, a field in itself whose literature is immense. The model however, is amenable to solution by simulation; and that makes it, as is often the case, quite instructive.

First we find, by means of an adequate MC protocol, that there is an equilibrium first order phase transition between the two states, with the correct Pauling entropy jump and an instructive proton ring distribution in the FE and PE states. The equilibrium transformation between the two does not take place by regular nucleation as in normal first order transitions because, as is known for a very long time, IRs make ordinary nucleation[50] ineffective: leaving pure, defect free bulk ice in a metastable PE state endowed by Pauling's entropy and a very characteristic proton ring distribution down to the lowest temperatures.

By introducing impurities, mimicking dopants such as KOH known experimentally to nucleate the transition, we examine the very special FE-PE and PE-FE heterogeneous nucleation mechanism in an IR-obeying system . The dopant generates an itinerant hydroxide-induced defect whose string-like evolution inside the bulk effectively punctures, as it were, the otherwise infinite barrier between the two states, ending the kinetic invulnerability of the metastable PE state at low temperatures. Starting with the PE state, the growth of the hydroxide string provides a quasi one-dimensional heterogeneous nucleation mechanism, with a propagating winding cloud of FE rings inside the initially proton-disordered bulk. This is in turn reflected by the increase of the FE order parameter as time (in our case MC time) evolves after quenching, as simulations show (Fig. 2(a)). Snapshots in Fig. 4 (and Fig. 3) moreover show a predicted FE (PE) nucleation landscape proceeding along the string of flipped protons which acts as the backbone. These strings and in fact the qualitative nature of the nucleation process are reminiscent of Kasteleyn-like transitions in spin ice models– not surprisingly, because the ordered (disordered) phase onset is again IR-dominated[30]. Nonetheless, the differences are important. Already at equilibrium, Fig. 1(d) compares the temperature dependence of the order parameter of the ice model with that of a spin ice model

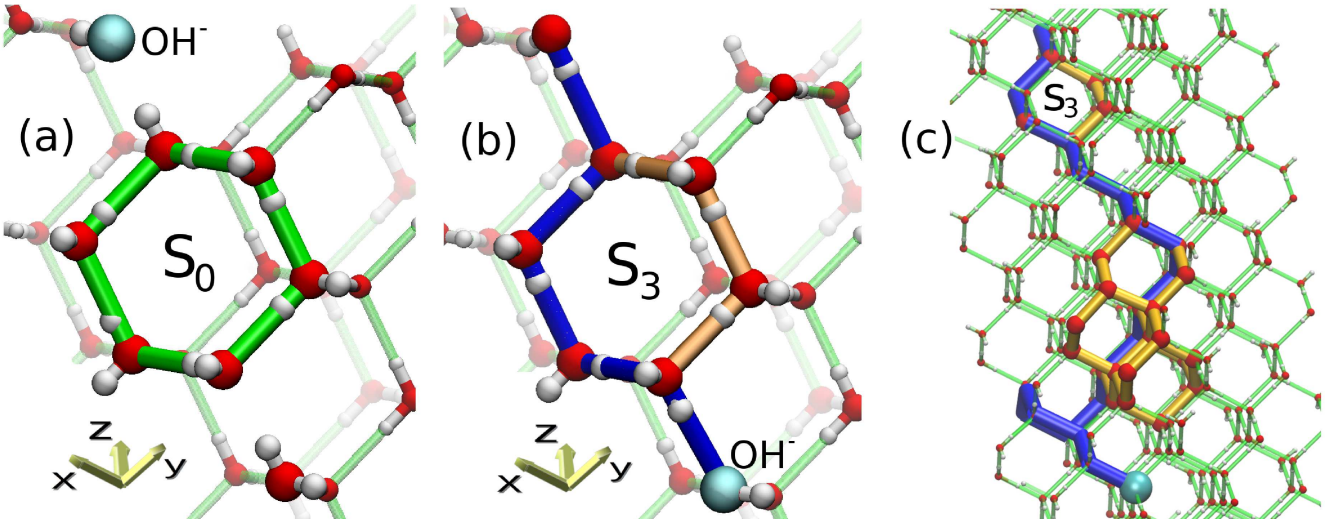

Figure 4: Nucleation mechanism of FE clusters inside the PE phase of ice depicted with snapshots of the simulation at different stages of the process (see explanations in *Microscopic Mechanism of String Nucleation*): (a) After thermalization at $T = 3T_c$ showing the hydroxide defect (colored with turquoise) and different "disordered" green rings; (b) immediately after quenching below T_c showing the blue path of the hydroxide and the consequent conversion of a (green) S_0 ring into a z-polarized S_3 (mustard) ring; (c) after a longer simulation time at $T < T_c$ showing the blue path of the hydroxide. In its travel, the hydroxide nucleates a new mustard S_3 cluster (shown at the top of the image) and enables to enlarge an already existing FE mustard cluster (shown at the bottom of the image).

(see Gohlke *et al.*[42]) with the same IRs but with an external field instead of our local dipole-dipole interaction (i.e., with $J = 0$ in our language). In spin ice there is a 3D Kasteleyn transition in the low-field regime with a characteristic second-order behavior at $T > T_c$, in contrast to the first-order behavior of our phase transition. Beyond that, the evolution kinetics of strings in our ice model is controlled by J, again an element absent in spin ice models.

A number of results suggested by the present lattice ice model encouragingly resemble those known either experimentally or in more elaborate off-lattice models of water ice.

The static structure and ring correlations and the correct Pauling entropy of clean bulk ice appear to describe well the disordered PE state, as summarized by Fig. 1. The capability of metal hydroxide dopants to give rise to growing FE strings inside the PE state and viceversa – thus functioning as unconventional inhomogeneous nucleation agents – is demonstrated, as in Figs. 3 and 4. The long-time FE polarization fraction grows as the quenching temperature increases approaching T_c (Fig. 2(b)), in nontrivial agreement with neutron diffraction experiments and contrary to usual ferrodistortive structural transitions where clusters with reversed order parameters below T_c lead to a decrease of the average order parameter as T increases approaching the transition[51–53]. Again similar to real ice, the dependence of FE polarization upon the dopant concentration is minimal. In the model, inhomogeneous nucleation occurs with any number of extrinsic centers, and the residual increasing effectiveness appears simply to reflect a speed-up kinetics once the system is close to the transition point. Finally, the slowing down in the growth rate of FE polarization order parameter with MC time also resembles that observed in water ice in real time– see Fig. 2. In that slowing down however a multiplicity of elements can be simultaneously at work. The string nuclei cannot, owing to their nanoscale transverse size, convert, in a system with strict IRs, a PE state to complete ferroelectricity. Probably even more important in practice, string nuclei might suffer a decrease of their growth rate when their tips hit other existing FE clusters, or, in real ice, grain boundaries and other lattice defects. In our simulations, that kind of effect is involuntarily introduced by finite size. Even ignoring these important realistic aspects, one could note that the partially polarized system free energy is progressively closer to the FE equilibium state than the disordered starting point, yielding a decreasing thermodynamic force felt by the growing string tip ends.

Beyond purely on-lattice models like ours, the moving hydroxide can, besides moving on in-lattice configurations[27,28], also visit (and be arrested by) off-lattice interstitial configurations[29]. That event, not described in our model, will slow down the hydroxide mobility and also introduce kinks with possible bifurcations in the strings evolution. An evolution which nevertheless our model depicts in its most elementary form.

In conclusion, we have presented a soluble lattice model depicting the onset of ice ferroelectricity as a first order phase transition, and demonstrating how nucleation and growth mechanisms, otherwise universal in the kinetics of first order phase transitions, are profoundly changed by topological ice-rule constraints that control

proton ordering. Results sheds light on, and support further understanding of, the onset and demise of ferroelectricity in ice.

Acknowledgments

E.T. thanks R. Car and S. Singer for very helpful discussions and inputs. J.L. and S.K. acknowledge fruitful discussions with S. Scandolo. J.L. also thanks A. Hassanali for helpful suggestions. J.L. and S.K. acknowledge support from Consejo Nacional de Investigaciones Científicas y Técnicas (CONICET), Argentina. E.T. is supported by ERC Advanced Grant N. 8344023 ULTRADISS, and in part by the Italian Ministry of University and Research through PRIN UTFROM N. 20178PZCB5.

[1] J. D. Bernal and R. H. Fowler, J. Chem. Phys. **1**, 515 (1933).
[2] A. Rahman and F. H. Stillinger, J. Chem. Phys. **57**, 4009 (1972), https://doi.org/10.1063/1.1678874, URL https://doi.org/10.1063/1.1678874.
[3] V. F. Petrenko and R. W. Whitworth, *Physics of Ice* (Oxford University Press, Oxford, 1999).
[4] L. Pauling, J. Am. Chem. Soc. **57**, 2680 (1935).
[5] S. T. Bramwell, Nature **397**, 212 (1999).
[6] K. Umemoto, Rev. Mineral. Geochem. **71**, 315 (2010).
[7] X. Su, L. Lianos, Y. R. Shen, and G. A. Somorjai, Phys. Rev. Lett. **80**, 1533 (1998), URL https://link.aps.org/doi/10.1103/PhysRevLett.80.1533.
[8] T. Sugimoto, N. Aiga, Y. Otsuki, K. Watanabe, and Y. Matsumoto, Nature Physics **12**, 1063 (2016).
[9] Y. Tajima, T. Matsuo, and H. Suga, Nature **299**, 810 (1982).
[10] Y. Tajima, T. Matsuo, and H. Suga, J. Phys. Chem. Solids **45**, 1135 (1984).
[11] H. Fukazawa, M. Arakawa, H. Yamauchi, Y. Sekine, R. Kobayashi, Y. Uwatoko, S. Chi, and J. A. Fernendez-Baca, JPS Conf. Proc. **8**, 033010 (2015).
[12] H. Fukazawa, S. Ikeda, M. Oguro, T. Fukumura, and S. Mae, J. Phys. Chem. B **106**, 6021 (2002).
[13] H. Fukazawa, A. Hoshikawab, H. Yamauchib, Y. Yamaguchic, and Y. Ishiib, J. Cryst. Growth **282**, 251 (2005).
[14] S. Koval, J. Kohanoff, R. L. Migoni, and E. Tosatti, Phys. Rev. Lett. **89**, 187602 (2002), URL https://link.aps.org/doi/10.1103/PhysRevLett.89.187602.
[15] B. Pamuk, P. B. Allen, and M.-V. Fernández-Serra, Phys. Rev. B **92**, 134105 (2015).
[16] D. Donadio, P. Raiteri, and M. Parrinello, J. Phys. Chem. B **109**, 5421 (2005).
[17] S. J. Singer, J.-L. Kuo, T. K. Hirsch, C. Knight, L. Ojamäe, and M. L. Klein, Phys. Rev. Lett. **94**, 135701 (2005), URL https://link.aps.org/doi/10.1103/PhysRevLett.94.135701.
[18] M. Schönherr, B. Slater, J. Hutter, and J. VandeVondele, J. Phys. Chem. B **118**, 590 (2014).
[19] Z. Raza, D. Alfe, C. G. Salzmann, J. Klimeš, A. Michaelides, and B. Slater, Phys. Chem. Chem. Phys. **13**, 19788 (2011).
[20] P. Geiger, C. Dellago, M. Macher, C. Franchini, G. Kresse, J. Bernard, J. N. Stern, and T. Loerting, J. Phys. Chem. C **118**, 10989 (2014).
[21] V. Buch, P. Sandler, and J. Sadlej, J. Phys. Chem. B **102**, 8641 (1998).
[22] S. W. Rick, J. Chem. Phys. **122**, 094504 (2005).
[23] G. T. Barkema and J. de Boer, J. Chem. Phys. **99**, 2059 (1993).
[24] J. Lekner, Physica B **240**, 263 (1997).
[25] J. Lekner, Physica B **252**, 149 (1998).
[26] G. Tribello and B. Slater, Chemical Physics Letters **425**, 246 (2006).
[27] C. Knight, S. J. Singer, J.-L. Kuo, T. K. Hirsch, L. Ojamäe, and M. L. Klein, Physical Review E **73**, 056113 (2006).
[28] C. Knight and S. J. Singer, Kuhs, W. F. (Ed.) Physics and Chemistry of Ice, The Royal Society of Chemistry p. 339 (2007).
[29] L. Cwiklik, J. P. Devlin, and V. Buch, J. Phys. Chem. A **113**, 7482 (2009).
[30] C. Castelnovo, R. Moessner, and S. Sondhi, Annu. Rev. Condens. Matter Phys. **3**, 35 (2012).
[31] P. W. Kasteleyn, J. Math. Phys. **4**, 287 (1963).
[32] L. D. C. Jaubert, J. T. Chalker, P. C. W. Holdsworth, and R. Moessner, Nature Physics **5**, 258 (2009).
[33] M. V. Ferreyra, G. Giordano, R. A. Borzi, J. J. Betouras, and S. A. Grigera, Eur. Phys. J. B **89**, 51 (2016).
[34] N. Bjerrum, Science **115**, 385 (1952).
[35] R. G. Melko and M. J. P. Gingrass, J. Phys.: Condens. Matter **16**, R1277 (2004).
[36] B. C. den Hertog and M. J. P. Gingras, Phys. Rev. Lett. **84**, 3430 (2000), URL https://link.aps.org/doi/10.1103/PhysRevLett.84.3430.
[37] S. Bramwell and M. Gingras, Science **294**, 1495 (2001).
[38] A. Bunker and B. Dünweg, Phys. Rev. E **63**, 016701 (2000), URL https://link.aps.org/doi/10.1103/PhysRevE.63.016701.
[39] R. Affentranger, I. Tavernelli, and E. E. Di Iorio, J. Chem. Theory Comput. **2**, 217 (2006), URL https://doi.org/10.1021/ct050250b.
[40] K. Hukushima and K. Nemoto, J. Phys. Soc. Jpn. **65**, 1604 (1996), https://doi.org/10.1143/JPSJ.65.1604, URL https://doi.org/10.1143/JPSJ.65.1604.
[41] F. Y. Wu, Rev. Mod. Phys. **54**, 235 (1982), URL https://link.aps.org/doi/10.1103/RevModPhys.54.235.
[42] M. Gohlke, R. Moessner, and F. Pollmann, Phys. Rev. B **100**, 014206 (2019), URL https://link.aps.org/doi/10.1103/PhysRevB.100.014206.
[43] A. Hassanali, F. Giberti, J. Cuny, T. D. Kühne, and M. Parrinello, Proc. Natl. Acad. Sci. **110**, 13723 (2013), ISSN 0027-8424, https://www.pnas.org/content/110/34/13723.full.pdf, URL https://www.pnas.org/content/110/34/13723.
[44] C. P. Herrero and R. Ramírez, J. Chem. Phys. **140**, 234502 (2014).
[45] M. Tyagi and S. S. N. Murthy, J. Phys. Chem. A **106**, 5072 (2002), https://doi.org/10.1021/jp012097x, URL https://doi.org/10.1021/jp012097x.
[46] C. Castelnovo, R. Moessner, and S. Sondhi, Nature **451**, 42 (2008).

[47] M. J. P. Gingras, Science **326**, 375 (2009).
[48] D. J. P. Morris, D. A. Tennant, S. A. Grigera, B. Klemke, C. Castelnovo, R. Moessner, C. Czternasty, M. Meissner, K. C. Rule, J.-U. Hoffmann, et al., Science **326**, 411 (2009).
[49] L. D. C. Jaubert, J. T. Chalker, P. C. W. Holdsworth, and R. Moessner, Phys. Rev. Lett. **100**, 067207 (2008).
[50] D. Kashchiev, *Nucleation: Basic Theory with Applications* (Butterworth-Heinemann, Oxford, 2000).
[51] T. Schneider and E. Stoll, Phys. Rev. B **17**, 1302 (1978), URL https://link.aps.org/doi/10.1103/PhysRevB.17.1302.
[52] T. Schneider and E. Stoll, Phys. Rev. B **13**, 1216 (1976), URL https://link.aps.org/doi/10.1103/PhysRevB.13.1216.
[53] V. Yukalov, Phys. Rep. **208**, 395 (1991).